TITLE: Breaks *invisible* to the DNA damage response machinery accumulate in ATM deficient cells

AUTHORS: Marta Martín[1,2], Mariona Terradas[2], George Iliakis[3], Laura Tusell[2] and Anna Genescà[1,2]

[1]Institute of Biotechnology and Biomedicine and [2]Department of Cell Biology, Physiology and Immunology, Universitat Autònoma de Barcelona, 08193 Cerdanyola del Vallès, Barcelona, Spain; [3]University Duisburg-Essen Medical School, 45122 Essen, Germany

RUNNING TITLE: *Invisible* breaks accumulate in AT cells

KEYWORDS: ATM; radiosensitivity; chromosome breaks; DNA damage response; γH2AX-labelling

ABSTRACT

After irradiation ATM defective cells accumulate unrepaired DSBs for several cell divisions. At the chromosome level, unresolved DSBs appear as chromosome breaks that can be efficiently scored by using telomeric and mFISH probes. H2AX is immediately activated by ATM in response to DNA damage and its phosphorylated form, γH2AX, flanks the DSB through several megabases. The γH2AX-labelling status of broken chromosome ends was analysed in AT cells in order to check whether the DNA damage response was accurately taking place in these persistent DSBs. The results show that one quarter of the scored breaks are devoid of γH2AX foci in ATM deficient cells metaphase spreads, and this fraction is significantly higher than in normal cells (χ^2<0,05). Accumulation of sensor and repair proteins at damaged sites is a key event in the cellular response to DSBs, so Mre11 labelling at broken ends was also analysed. While all γH2AX foci scored at visible broken ends co-localize with Mre11 foci, all γH2AX-unlabelled breaks are also devoid of Mre11-labelling. The present results suggest that a significant subset of the AT long-lived DSBs may persist as *invisible* DSBs due to deficient detection by the DNA damage repair machinery. While properly signalled DSBs will eventually be repaired; *invisible* breaks may indefinitely accumulate, most probably contributing to the AT cells' well known genomic instability.

217 words

INTRODUCTION

Failure to repair double strand breaks (DSBs) leads to genomic instability due to the loss of genetic material and the generation of deleterious mutations that contribute to oncogenesis. One of the main players involved in cellular responses to DNA-damage is the Ataxia Telangiectasia Mutated (ATM) protein, which belongs to the highly conserved PI3K-like protein kinase family (PIKKs). ATM plays an important role as a transducer and amplifier of the damage signal (Abraham and Tibbetts, 2005; Kurz and Lees-Miller, 2004; Shiloh, 2006), and phosphorylates many proteins involved in DNA-repair and cell cycle-checkpoint activation, thus providing the initiating steps of the DDR (DNA damage response) machinery.

One of the earliest responses to DNA damage is the phosphorylation of a highly conserved histone variant, H2AX, yielding a modified form called γH2AX (Rogakou et al., 1998), which spreads over at least 2Mb from the DSB site (Rogakou et al., 1999). γH2AX is reported to recruit numerous DSB-repair proteins and DNA damage-sensors involved in DNA repair, as well as chromatin remodelling factors and cohesins (Celeste et al., 2003; Paull et al., 2000; Ward et al., 2003). After the exposure of cells to IR, histone H2AX phosphorylation occurs rapidly, and reaches a maximum 30-60 minutes later (MacPhail et al., 2003; Rogakou et al., 1999). It is generally believed that the number of γH2AX foci reflects the number of DSBs generated in the genome (Rogakou et al., 1999; Rothkamm and Lobrich, 2003; Sedelnikova et al., 2002). Although most of these DSBs are repaired within minutes, a few can remain unrepaired for longer periods, even weeks (Kühne et al., 2004). It is believed that these persistent γH2AX foci represent unrejoined DSBs (Ichijima et al., 2005), which makes γH2AX a useful marker for residual DSBs in irradiated cells. Even though ATM is one of the main kinases involved in H2AX phosphorylation after exposure to IR (Burma et al., 2001), γH2AX foci are actually formed in AT cells, as they are also formed in DNA-PKcs defective cells (Ichijima et al., 2005; Kato et al., 2006; McManus and Hendzel, 2005; Rogakou et al., 1999). Thus, H2AX

phosphorylation appears to be a highly significant and evolutionarily conserved cellular response to DSBs, and the lack of one of the kinases involved in its phosphorylation is compensated by the activity of the remaining kinases (Stiff et al., 2004).

Defects in ATM underlie the autosomal recessive disorder ataxia-telangiectasia (AT). Cells from affected individuals are highly sensitive to IR and radiomimetic drugs. Historically, an increased frequency of residual chromosome breaks has been described in irradiated AT as compared to normal cells at the first mitosis after irradiation (Cornforth and Bedford, 1985). Subsequent work analysing chromosome aberration spectra obtained from irradiated AT cells yielded similar results, and an increased frequency of unrejoined chromosome breaks was described as an important contributor to AT cells radiosensitivity (Kawata et al., 2003; Martín et al., 2003). The above data is reinforced by results obtained after analysing DSBs rejoining kinetics in AT cells using pulsed field gel electrophoresis and γH2AX foci scoring (Foray et al., 1997; Kühne et al., 2004). Both techniques have provided clear evidence that failure to repair a subset of radiation-induced breaks -which remain unrepaired for long post-irradiation times-, is a hallmark of ATM deficient cells.

The accumulation of unresolved DSBs could underlie the severe radiosensitivity of AT cells, and their repair defect could be intimately linked to the nature of these persistent breaks. Several studies have sought to unravel any special characteristics of these DSBs and find out how the repair machinery interacts with them. It has been reported that ATM-induced Artemis activity may be involved in the resolution of a fraction of radiation-induced breaks. In AT cells, these breaks would remain unrepaired for long post-irradiation times (Jeggo and Lobrich, 2005; Riballo et al., 2004). Very recent data also suggests that ATM deficiency may render some breaks located at heterochromatic regions less accessible to the repair machinery (Goodarzi et al., 2008). Finally, after analysing ATM functions in V(D)J recombination, some authors suggested

a role of ATM in stabilizing DNA DSBs repair complexes, facilitating prompt and correct repair (Bredemeyer et al., 2008; Bredemeyer et al., 2006). However, to date no conclusive results have been obtained, and the specific nature -if any- of these breaks remains uncertain.

In the present work we investigate the induction and rejoining of DNA DSBs and analyze the properties of apparently terminal deletions in consecutive cell divisions in irradiated AT and normal lymphoblastoid cells. We reasoned that cytologically analysing visible broken DNA ends could provide further insight into the characteristics of these persistent breaks and how the repair machinery behaves in them. Many studies analysing γH2AX foci induction after IR have been performed on interphase cell nuclei, which make it impossible to distinguish γH2AX foci that signal DSBs from γH2AX foci emerging as a consequence of other processes such as cell cycle-dependent telomere uncapping, telomere dysfunction or replication stress. To prevent these ambiguities we used a combination of γH2AX immunofluorescence and telomeric-FISH on chromosomes from metaphase spreads, which enabled us to establish a direct link between a chromosome break and a γH2AX focus. Our results demonstrate that AT cells present γH2AX-labelled broken chromosome ends at a higher frequency than control cells, confirming that the persistence of unrejoined chromosome breaks is a hallmark of AT cells. Remarkably, a fraction of visible chromosome breaks lacks γH2AX as well as Mre11 signalling, this fraction being significantly higher in AT cells. Absence of signalling and repair protein foci on these breaks suggests inefficient detection by the DDR machinery and, as a consequence, they accumulate through subsequent cell divisions devoid of repair.

RESULTS

1. An excess of broken, unrejoined chromosomes is a hallmark of irradiated AT lymphoblasts several divisions after irradiation

Our previous work demonstrated that at first division after exposure to 1 Gy γ-rays, AT cells exhibited a significantly higher frequency of broken and unrejoined chromosomes than normal cells (Martín et al., 2003). The first aim of the present study was to determine whether these chromosome breaks are eventually repaired or whether they remain unresolved at further divisions p.i. Metaphase spreads from AT and normal cells were therefore analyzed at 71h p.i., a time where metaphases at second and third division p.i. were scored. Telomeric and centromeric FISH followed by mFISH was applied, thus unresolved breaks and other chromosome aberrations were unambiguously identified. The results obtained indicate that even after two or three cell divisions, the frequency of aberrant metaphases is higher in AT (65.0%) than in normal cells (46.7%) (χ^2 p=0,01) (Table 1), and the frequency of total chromosome aberrations is more than double in AT cells (1.833 aberrations/cell) than in normal ones (0.833 aberrations /cell) (Table 1), reflecting the greater radiosensitivity of ATM deficient cells

Chromosome aberrations were divided into exchange-type aberrations (including translocations, dicentrics and rejoined interstitial deletions), and non-exchange-type aberrations (including unrejoined chromosome breaks as well as terminal and unrejoined interstitial deletions) (Table 1 and Figure 1A). At 2nd and 3rd division p.i., exchange-type aberrations are the most frequent class of chromosome aberration observed, both in AT (1.300 exchange aberrations/cell) and in normal cells (0.710 exchange aberrations/cell), but neither individual nor grouped analysis of the exchange-type aberrations yielded a statistically significant difference between both cell types (Table 1). Regarding non-exchange type aberrations, the frequency of chromosome breaks and terminal deletions was 7 times higher in irradiated AT than in normal cells (0.467 *vs* 0.071 respectively; χ^2 test, $p<0.0001$). Since each unrejoined break generates two ends, we determined

the total number of broken ends remaining open at this point in time (Table 2). Irradiated AT cells presented 0.983 open ends/cell, more than 6 times the frequency of normal cells, where 0.152 open ends/cell were scored. Therefore, while normal cells have repaired most of the radiation-induced breaks and accumulate mostly exchange-type aberrations; 30% of the radiation-induced aberrations in AT cells remain unrejoined at 2nd and 3rd division p.i. These results confirm that although AT cells sustain a substantial capacity for repair , they fail to repair a significant fraction of radiation-induced breaks, which remain unrepaired after several cell divisions.

2. Sister Chromatid Fusion does not seal broken chromosomes in AT cells.

When performing the cytogenetic analysis described above we observed that, occasionally, chromosomes in irradiated AT cells presented apparently rounded and continuous ends, as if their sister chromatids had fused to adopt a ring-like shape. If the sister chromatids of a broken chromosome fuse and form a loop, many of the chromosome ends without telomeric signals that were recorded as breaks will actually reflect repair events. This mechanism has been described in mouse embryonic stem cells and cancer cell lines lacking p53-dependent G1 cell cycle checkpoint (Lo et al., 2002a; Lo et al., 2002b). Checkpoint defects in these cells allowed them to progress through the cell cycle with unrepaired chromosomes. In the S phase, the broken chromatid will duplicate and can fuse to its newly synthesized sister chromatid. Thus, given the associated cell-cycle checkpoint defect AT cells present, it is theoretically possible that these cells could find in the fusion of sister chromatids (SCF) a mechanism to seal a fraction of unrepaired breaks. To ascertain whether broken chromosomes accumulating in AT cells remain truly open, chromosomes presenting rounded ends and corresponding to first division p.i. were identified in AT and normal cells. Afterwards, a telomeric probe was applied and the absence of telomeric signals at a previously detected rounded end was interpreted to be an SCF event. The results (Figure 2A) suggest that, for the cell types used here, this analysis is not specific enough

(as confirmed by the telomeric FISH), since an important number of false positives is detected (Figure 2A). To conclusively clarify this issue, we looked for the expected cytogenetic outcomes of SCF events: isodicentric or isoacentric chromosomes showing the typical mirror-banding pattern. These rearrangements are the direct result of an SCF event which has evolved and persisted through at least two cell divisions (Figure 2B). Analysis of metaphases corresponding to 2nd, 3rd and further divisions p.i. (48, 71 and 141 h p.i) using mFISH reveals only a few iso-aberrations (Figure 2C) in either cell type. This result leads us to conclude that SCF does not play a role in repairing broken ends in AT cells. Therefore, most of the unrejoined breaks scored in the previous cytogenetic analysis should be considered uncapped broken ends that remain open.

3. DSBs rejoining kinetics is similar in AT and normal cells, but more DSBs may remain unrepaired in AT cells

Possible explanations for the higher yields of chromosome breaks in AT cells are a higher induction or a diminished repair of IR induced DSBs. We therefore tested induction and rejoining of DSBs in irradiated normal and AT lymphoblasts by Asymmetric Field Inversion Gel Electrophoresis (AFIGE). To our knowledge, information regarding induction and rejoining kinetics of DSBs in AT cells is only available for fibroblasts (Foray et al., 1997; Kühne et al., 2004; Löbrich et al., 2000), and it is in principle possible that lymphoblasts show a different response. The results in Figure 3 indicate that DSB induction is similar in AT and normal cells. Also, the kinetics of DSB rejoining is similar between AT and normal cells over a period of 8 hours after 30 Gy of radiation. However, at longer times post-irradiation AT cells appear to have a larger fraction of unrejoined DSBs. Although the difference does not reach statistical significance in our experiments (Figure 3B), numerous studies of DSB repair in AT fibroblasts confirm this observation (Blöcher et al., 1991; Foray et al., 1997; Kühne et al., 2004). In conclusion, our results rule out increased induction or delayed rejoining of DSBs as a cause for

the accumulation of chromosome breaks and, instead, suggest a failure to rejoin a fraction of the generated DSBs as the cause of radiosensitivity in AT cells.

4. AT cells show defects in H2AX phosphorylation in a fraction of chromosome breaks

Accumulation of broken chromosomes in AT cells at different cell divisions p.i. raises the question of whether these breaks are being correctly sensed. A physiologically important downstream target of ATM is H2AX, which is rapidly phosphorylated to concentrate repair proteins in the vicinity of DSBs. We decided to examine whether the absence of functional ATM leads to defective signalling of DSBs by γH2AX, which might in turn compromise repair. To ascertain whether γH2AX foci formation occurs in AT cells at the same efficiency as in normal cells, we used telomeric-FISH to identify breaks in metaphase chromosomes and tested them for γH2AX signal presence. Metaphase spreads at first and second division p.i. were obtained from normal and AT cells. Chromosome breaks were identified as broken centric or acentric fragments that had telomeric signals only on one end. In agreement with the above cytogenetic analysis and with AFIGE results, a higher frequency of breaks is scored in irradiated AT than in normal cells (0.937 *vs* 0.429 breaks/cell, respectively) (Table 3). Of these chromosome breaks the vast majority (0.367 out of 0.438 breaks/cell) displayed γH2AX signal in normal cells, and a significant fraction (0.691 out of 0.937 breaks/cell) in AT cells (Table 3 and Figure 4A). Thus, γH2AX is detectable on most chromosome ends lacking telomeric signals, indicating that they reflect broken chromosome ends which are still open. A significantly higher fraction of γH2AX-labelled breaks is scored in AT cells in comparison to normal ones. These results are in accordance with γH2AX foci kinetic analysis performed in interphase cell nuclei, which report a slower disappearance of γH2AX foci in AT cells (Karlsson and Stenerlöw, 2004; Kato et al., 2006). The slower disappearance reflects persistent DSBs that wait for efficient repair in ATM deficient cells, and these persistent DSBs are clearly identified in our work as γH2AX-labelled broken chromosomes. In short, the present results confirm that persistence of unrepaired breaks

is a hallmark of AT cells; and, although still unresolved, most of these breaks are being correctly sensed by the DNA damage repair machinery.

Surprisingly, and as inferred from the results described above, breaks devoid of γH2AX signal are also found, and they are more frequently observed in AT than in normal cells (Table 3 and Figure 4A). In addition, the fraction of chromosome breaks without γH2AX signal in normal cells is similar before and after irradiation (20.00% and 15.95% respectively) and it is also similar in AT cells (27.77% before irradiation and 26.25% after irradiation), suggesting that break-labelling is independent of radiation exposure. Therefore, we computed together all the breaks scored before and after irradiation and classified them on the basis of their γH2AX labelling status (Table 3 and Figure 4C). The pooled results show that 26.4% of chromosome breaks are devoid of γH2AX foci in AT cells, while only 16.5% of the breaks lacked γH2AX in normal cells (χ^2, $p<0,05$). Thus, AT cells display a significantly higher fraction of γH2AX-unlabelled chromosome breaks. In order to further characterize these unlabelled breaks, mFISH was applied to the same slides. Most of the γH2AX-labelled breaks (61%) corresponded to chromatid or chromosome breaks in which both ends of the broken chromosomes (same colour fragments) were present in the cell (Figure 4B). Instead, γH2AX-unlabelled centric or acentric fragments frequently appeared without the complementary fragment of the chromosome (Figure 4C), suggesting that cells carrying γH2AX-unlabelled breaks have overcome the first division after irradiation.

5. DSBs without γH2AX remain invisible to the DDR machinery

The above observations suggest that some of the scored breaks are not efficiently sensed by the DDR machinery, and thus their repair may be compromised. To definitively clarify whether an absence of γH2AX foci actually reflects a defect in the recruitment of repair factors to breakpoints, immunofluorescent detection of γH2AX together with Mre11 was applied to

metaphase chromosome preparations. Mre11 belongs to the MRN complex together with Nbs1 and Rad-50, and it is known to be recruited to the DSBs very soon after damage is inflicted, where it actively participates in DNA DSB recognition and repair (Lavin, 2007; Lee and Paull, 2007; Williams et al., 2007). The results show that γH2AX foci in breakpoints clearly co-localize with Mre11 foci, indicating that the break has been detected and that repair is taking place at the DSB (Figure 5A). However, breaks devoid of γH2AX-label also lack the Mre11 foci (Figure 5A), indicating a lack of recruitment of DSB repair proteins to γH2AX-unlabelled breaks.

In the hypothetical case that the absence of γH2AX-signalling was due to technical limitations or because the signal was below the detection limit, the fraction of breaks devoid of γH2AX foci would be similar in both cell types. However, in this analysis, AT cells display a higher fraction of γH2AX- and Mre11-unlabelled breaks than normal cells (Figure 5B). In addition, all γH2AX-unlabelled breaks are always Mre11-unlabelled and vice versa. If the technique had detection defects, some breaks would appear unlabelled in a random distribution. Hence, the labelling pattern of the two different repair proteins described here can be considered not to be random in nature, as well as being significant and clear evidence that the lack of γH2AX-labelling implies the absence of recruitment of additional repair proteins at the affected breaks. Altogether the present results suggest that a hallmark of AT cells is the accumulation of an important fraction of breaks that lack both γH2AX- and Mre11-labelling. It could be argued that these breaks are somehow capped. Hairpin structures could potentially seal these broken chromosomes and this event would explain the deficiency in γH2AX-and Mre11-signalling. Although we cannot exclude this possibility, hairpin resolution during V(D)J coding end formation is not impaired in ATM deficient cells (Niewolik et al., 2006), which suggests that AT cells are able to repair this kind of structure. Therefore, the absence of any recruitment of repair factors to these breaks renders them *invisible* to the cell repair machinery. If not efficiently sensed, these breaks can accumulate in an unrepaired state through subsequent cell divisions.

DISCUSSION

The work presented here demonstrates that unrejoined chromosome breaks are a hallmark of lymphoblastoid AT cells that may contribute to their exacerbated radiosensitivity. An excess in unrepaired chromosome breaks is observed in AT cells in the 1st, 2nd and 3d divisions after irradiation analysed. The DNA DSB rejoining kinetic analysis rules out increased DSB induction and slower DSB rejoining kinetics as causes of the accumulation of unrepaired chromosome breaks in AT cells. These results also demonstrate that although AT lymphoblasts display a significant DSB repair capacity, they are unable to repair a fraction of the induced DSBs, which persist -in close accordance with our cytogenetic results- through subsequent cell divisions. Very similar rejoining kinetics have been described before in AT fibroblasts (Foray et al., 1997; Kühne et al., 2004; Löbrich et al., 2000), and it has been proposed that a fraction of the IR-induced breaks are refractory to efficient repair in AT cells. Given the present results we inquired whether defects in sensing chromosome breaks could underlie unresolved breaks accumulation.

Considering that ATM is one of the main kinases involved in H2AX phosphorylation, an appropriate first step appeared to involve checking the broken chromosome ends for γH2AX-labelling. The developed technique allows unequivocal identification of γH2AX foci specifically associated with previously scored broken chromosome ends. First of all, the results demonstrate that AT cells accumulate more unrepaired breaks than normal cells, and 75% of them display a γH2AX focus on their broken end. It has previously been described that in ATM deficient cells, DNA-PKcs kinase may serve to phosphorylate H2AX after IR (Stiff et al., 2004). Because AT cells accumulate more breaks than normal cells, and 75% of these breaks are γH2AX-labelled, more γH2AX-foci are scored in AT cells at all times analysed. This result is in line with studies that report a slower disappearance over time of γH2AX foci in irradiated AT cells (Karlsson and Stenerlöw, 2004; Kato et al., 2006; Kühne et al., 2004; Rogakou et al., 1999). Slower

disappearance of γH2AX foci suggests that the absence of ATM favours the persistence of broken chromosomes awaiting efficient repair. Our results are also consistent with recent studies of mouse peripheral blood lymphocytes, which report that most aberrations displayed by *Atm*$^{-/-}$ B cells are chromosome breaks (Franco et al., 2006) that remain unrepaired for several days (Callen et al., 2007).

Surprisingly, a fraction of the chromosome breaks scored in irradiated and non-irradiated AT and normal cells did not show a γH2AX signal at the broken ends, and this fraction was significantly higher in AT cells. To our knowledge, this is the first time that the absence of γH2AX-labelling has been described on visible broken chromosomes, suggesting that γH2AX-foci scoring may not precisely reflect all existing DSBs. It has been reported that H2AX phosphorylation is required to concentrate several repair factors in the vicinity of DNA lesions and provides correct assembly and retention at the break site (Celeste et al., 2003; Paull et al., 2000). The absence of γH2AX-labelling at certain breaks most probably implies the absence of additional repair factors, suggesting that the entire DDR cascade does not take place efficiently at these particular breaks. This statement is further corroborated by the Mre11-labelling pattern: while all γH2AX foci at broken chromosome ends co-localized with Mre11 foci, broken ends devoid of γH2AX-labelling also lacked Mre11-labelling. We propose that the fraction of chromosome breaks devoid of γH2AX foci lacks the "red flag" that alerts the DDR machinery to be uploaded and efficiently spread at a DSB. As a consequence, proper repair is hindered in a subset of IR-induced breaks.

Because γH2AX-unlabelled breaks are also scored in normal cells, one must assume that the presence of γH2AX-unlabelled breaks must result from a habitual process not related to a protein deficiency. In the present work, cells were analysed at first and second division p.i., and mFISH results suggest that γH2AX-unlabelled breaks are more commonly scored after the first cell division post-irradiation. It has recently been reported that cells can recover from the G2

checkpoint even in the presence of a few unrepaired DSBs (Krempler et al., 2007). Taken altogether, it is tempting to speculate that some unresolved breaks lose their γH2AX-mediated signalling as the cell proceeds through its cycle, maybe as a consequence of the extensive modifications that chromatin suffers when going through the different phases of the cell cycle. We speculate that breaks devoid of the γH2AX signal are initially labelled, but lose this labelling after several cell divisions despite being unrejoined, thus silencing the γH2AX-mediated signalling. In this context, both fast DSBs rejoining and correct cell cycle functioning are essential factors for avoiding accumulation of unrejoined breaks. ATM deficiency entails checkpoint and repair defects, and both characteristics would favour the accumulation of a significant amount of unrepaired breaks in comparison to normal cells. As AT cells continue to divide, a greater fraction of unresolved breaks would lose their γH2AX-labelling, accumulating in an unrepaired state.

Further work is needed to establish whether the initial formation of a γH2AX focus is defective in the affected breaks because of a DNA damage signal amplification defect or, alternatively γH2AX foci actually form, but this signalling decays as the cell resumes its cycle and before repair is completed. In any case, and regardless of its origin, the absence of proper γH2AX-labelling in unrepaired DSBs renders these breaks *invisible* to the DDR machinery. While properly signalled DSBs will eventually be repaired; a significant subset of the long-lived DSBs may remain *invisible* and accumulate in an unresolved state for an indefinite time. Thus, *invisible* breaks arise as a challenging source of genomic instability in ATM deficient cells.

MATERIAL AND METHODS

1. Cell culture and γ-ray exposure. The lymphoblastoid immortal cell lines GM08436A (AT) and GM09622, derived from an AT child and a matched control for sex and age, respectively, were obtained from the Coriell Cell Repositories. Both cell lines were grown in suspension in RPMI 1640 (GIBCO, BRL) medium and incubated in a 37ºC and 15% CO_2 atmosphere. Cells were irradiated with 1Gy γ-rays while exponentially growing using a CSL 15 R-^{137}Cs source (dose-rate: 6.14 Gy/min). Immediately after irradiation, BrdU (Sigma) was added to the culture at a final concentration of 12μg/ml in order to distinguish between post-irradiation divisions. Metaphase chromosome preparations were obtained at 24, 48, 71 and 144h after irradiation as described elsewhere (BrdU was added to the cell culture every 48 hours). Cells in the first, second, third and further cell divisions post-irradiation were determined by exposure to UV light of Hoechst 33258 (Sigma) treated slides (150μg/ml). Post-irradiation times presenting more than 90% of first divisions were chosen for SCF analysis. Post-irradiation times presenting more than 90% of second or further divisions were chosen for γH2AX and cytogenetic analysis respectively.

2. Fluorescent *in situ* hybridization (FISH). Unless otherwise specified, fluorescent signals were visualized under an Olympus BX 51 microscope using a 100X (Olympus) U Plan Apochromat lens (1.35 NA). The microscope was equipped with epifluorescence optics and a CV-M300 camera (MetaSystems GmbH.). Images were captured and analysed using Isis V5.0 software (FISH Imaging System, MetaSystems).

2.1 Telomeric and Centromeric FISH. Telomeric and centromeric hybridization was performed following the manufacturer's instructions using a Cy3-$(CCCTAA)_3$ PNA-probe for telomeres and a FITC-AAACACTCTTTTTGTAGA probe for centromeres (PE Biosystems). After PNA hybridization, DAPI counterstain was applied and images were captured and analysed using Isis V5.0 software (FISH Imaging System, MetaSystems).

2.2 Multiplex FISH (mFISH). After PNA-FISH, the same slides were used to perform multiplex FISH, in order to obtain the differential paintings of the whole set of chromosomes. The mFISH probe (Vysis, Inc.) containing five fluorochromes (Spectrum Gold™, Spectrum Aqua™, Spectrum FRed™, Spectrum Green™ and Spectrum Red™) was applied following the manufacturer's instructions. After mFISH hybridization and DAPI counterstaining, metaphases were relocated and re-captured using the Isis V5.0 software (FISH Imaging System, MetaSystems).

3. Cytogenetic analysis. Following metaphase capture, the mFISH hybridization pattern for each chromosome and each fragment was analyzed. Subsequently, the number of centromeric signals in each chromosome and fragment, and the number of telomeric signals at their natural ends were scored. A combination of mFISH and PNA-telomeric and -centromeric FISH enables exhaustive scoring of aberrations, giving highly accurate information about otherwise undetected breaks. The **simple aberrations** considered here were: *Dicentric chromosomes*: two-colour chromosomes with two centromeres. *Translocations*: two-colour chromosomes containing a single centromeric signal, resulting from the illegitimate joining of a centric fragment of a chromosome to an acentric fragment of a different chromosome. *Interstitial deletions*: one-colour chromosome broken at two distinct points, generating three fragments. *Chromosome breaks:* One-colour chromosome broken at one point, generating a centric fragment accompanied by the corresponding acentric fragment. *Terminal deletions*: One-colour chromosome broken at one point, with the peculiarity that one of the generated fragments is missing. For aberration type scoring, **complex aberrations** (those resulting from the exchange between two or more chromosomes that have suffered at least three breaks) were reduced to the simple aberration types described. All simple aberrations were classified as exchange type aberrations and non-exchange type aberrations. **Exchange type aberrations** included dicentrics, translocations and those interstitial deletions where two of the three generated fragments had

rejoined. **Non-exchange type aberrations** included chromosome breaks, terminal deletions and those interstitial deletions where the broken fragments remained unrejoined.

4. Scoring of aberrations. For each simple aberration, and after reducing complex aberrations to simple events, we scored as a single aberration the following combinations: **Dicentrics**: (1) each dicentric chromosome and the accompanying compound acentric fragment. (2) A dicentric chromosome accompanied by the two resulting unrejoined acentric fragments. (3) A compound acentric fragment (two colours) accompanied by the two unrejoined centric fragments. (4) A dicentric chromosome alone. (5) A compound acentric fragment alone. **Translocations**: (1) each translocated chromosome, together with its reciprocal translocation. (2) A translocated chromosome accompanied by the resulting unrejoined centric and acentric fragments. (3) A translocated chromosome alone. **Interstitial deletions**: (1) a centric or acentric fragment devoid of telomeric signals at both ends and accompanied by the two or three rejoined chromosome fragments of the same chromosome. (2) A centric or acentric fragment devoid of telomeric signals at both ends and accompanied by the two or three unrejoined chromosome fragments of the same chromosome origin. (3) A centric or acentric fragment devoid of telomeric signals at both ends alone**. Capping status**: An aberration was considered **rejoined** when a pair of telomeric signals was present at each end of the rearranged chromosomes. An aberration was considered **unrejoined** when at least one of the ends was devoid of telomeric signals. Statistical analysis was performed using GrapgPad Instat® software.

5. Sister chromatid fusion (SCF) analysis. Slides corresponding to first divisions after irradiation of normal and AT cells were selected and coded prior to any treatment, in order to perform a blind analysis. Slides were solid stained with Leishman, which strongly preserves the original chromosome morphology, thus providing a resolution tool to observe the fusion of chromatids. Centric and acentric fragments presumably forming SCF were identified by the

characteristic rounded aspect of one of their ends. Subsequently, telomeric-FISH was applied to the same slides and fragments with presumably fused chromatids scored in the solid-staining analysis were relocated. SCF events were actually confirmed when the previously detected rounded ends were devoid of telomere signals at the fusion point.

6. Asymmetrical field inversion gel electrophoresis (AFIGE). For the evaluation of DSB repair kinetics, AT and normal cells were cultured *in vitro* until both cell lines reached the *plateau* phase. Cells were cooled to 4ºC before irradiation and were irradiated on ice at 30Gy using a Pantak X-ray machine MXR-321, operated at 320 kV and 10 mA with a 1.6 mm Al filter. After irradiation, the cells were returned to the incubator at 37ºC to allow for repair. After each repair time interval, cells were centrifuged, washed with PBS, centrifuged again, and resuspended at a final concentration of $1x10^6$ cells/ml. Details of cell-agarose blocks preparation as well as the AFIGE have been previously described (Martín et al., 2005). The agarose gels were scanned immediately after electrophoresis and were quantified to estimate DNA damage using ImageQuant 5.2 (Amersham Biosciences Corp., Piscataway, NJ) software. DNA DSBs were quantified by calculating the fraction of activity released from the well into the lane (FAR) in irradiated and non-irradiated samples. The FAR measured in non-irradiated cells (background) was subtracted from the results shown in irradiated cells.

7. Immunofluorescence. After irradiation, cells were cultured for 48h and chromosome spreads were obtained as described by Jeppesen (Jeppesen, 2000). Briefly: cells were centrifuged and resuspended to a final concentration of $5x10^4$ cells/ml in a 1:1 proportion of cell culture medium and hypotonic solution (KCl 0,075M) supplemented with 0.1% Tween 20. Immediately thereafter, cells were cytocentrifuged and slides were washed with potassium chromosome medium (KCM) for 15min at room temperature (RT). After air drying, 15µl of blocking solution was applied to the slides (2% (v/v) serum in KCM) for 1h at RT. Both primary and secondary

antibodies were diluted in KCM containing 10% (v/v) serum. Slides were removed from KCM and 15µl of 1:800-diluted mouse anti-phospho-histone H2A.X (ser139) (Upstate) antibody was applied alone or together with 15 µl of 1:200-diluted rabbit anti-Mre11 (Abcam). Incubation was performed for 1h at 37ºC. Before secondary antibody incubation, the preparations were washed twice in KCM (5 min each) and the 1:400-diluted Alexa 488 and 1:1000-diluted Alexa 568 secondary antibodies (Molecular Probes; Invitrogen) were applied. After 40 minutes incubation at RT, the slides were washed for 2x5 min in KCM and fixed in KCM containing 4% (w/v) formaldehyde (15min). Finally, the preparations were briefly rinsed in distilled water and left to air dry. DAPI counterstain was applied to the slides and chromosome spreads were visualized and captured. In a correlative manner, a telomeric-FISH and an mFISH probe was applied to the same slides and metaphases were relocated and re-captured.

ACKNOWLEDGMENTS

This work was supported by grants from the European Union, Grant number FI-CT-2003-508842; Fundació *La Marató*, Grant number TV32005-050110; Ministerio de Educación y Ciencia, Grant numbers SAF2004-20372-E and SAF2006-01653; Instituto de Salud Carlos III, Grant number RD06/0020/1020; and Generalitat de Catalunya, Grant number 2005SGR-00437.

We thank the Language Advisory & Translation Unit at the Universitat Autònoma de Barcelona Language Service for editing the manuscript.

Table 1. Number, frequency and types of aberrations in normal and AT cells

		AT (freq/cell)		Normal (freq/cell)		χ^2
0Gy Irradiation	Cells analysed	31		69		
	Cells without aberrations	22	(0.709)	61	(0.884)	
	Cells with aberrations	9	(0.290)	8	(0.116)	-
	Chromosome Aberrations[1]	11	(0.355)	10	(0.145)	
	Exchange type aberrations[2]	1	(0.032)	-	-	
	Non-Exchange type aberrations[3]	10	(0.322)	10	(0.145)	-
1Gy Irradiation (71h p.i.)	Cells analysed	60		197		
	Cells without aberrations	21	(0.350)	105	(0.533)	
	Cells with aberrations	39	(0.650)	92	(0.467)	*p=0,01*
	Chromosome Aberrations[1]	110	(1.833)	166	(0.843)	
	Exchange type aberrations[2]	78	(1.300)	140	(0.710)	
	t	51	(0.850)	81	(0.411)	*n.s.*
	dic	23	(0.383)	52	(0.264)	*n.s.*
	R-id	4	(0.066)	7	(0.035)	*n.s.*
	Non-Exchange type aberrations[3]	32	(0.534)	26	(0.132)	*p<0,007*
	csb - del	28	(0.467)	14	(0.071)	*p<0,0001*
	UR-id	4	(0.066)	12	(0.061)	*n.s.*

[1]**Chromosome aberrations**: number of chromosome aberrations after reducing complex aberrations to simple aberrations (see material & methods section). No complex aberrations were scored in non-irradiated AT or normal cells. [2]**Exchange type aberrations: t:** translocations; **dic:** dicentrics; **R-id:** rejoined interstitial deletions; [3]**Non-exchange type aberrations: csb-del:** chromosome breaks and terminally deleted chromosomes; **UR-id:** unrejoined interstitial deletions. ***n.s.*:** non-significant. All frequencies shown in the table are calculated based on the total number of cells analysed.

Table 2. Breaks and chromosome open ends observed in normal and AT cells at 71h p.i.

	AT			Normal		
		MNB (freq/cell)	**ERO** (freq/cell)		**MNB** (freq/cell)	**ERO** (freq/cell)
Cells analysed	60			197		
Chromosome aberrations						
t	51	102	2	81	162	2
dic	23	46	1	52	104	-
R-id	4	8	-	7	14	-
csb - del	28	28	56	14	14	28
TOTAL	116	184 (3.066)	**59 (0.983)[a]**	154	294 (1.492)	**30 (0.152)[a]**

[a] ***6.5x difference***

MNB: Minimal Number of Breaks required to obtain the observed number of chromosome aberrations. *I. ex*: to generate a translocation or a dicentric, two breaks are needed; each on a different chromosome. These 2 breaks (MNB) will generate 4 open ends; **ERO**: Ends Remaining Open at a specific point in time. Visible ERO are detected and counted after applying the telomeric probe to the slides.

Table 3. Frequency of breaks with and without γH2AX signal

	Cells	Total Breaks (freq/cell)	Breaks **with** γH2AX signal (freq/cell)	Breaks **without** γH2AX signal (freq/cell)
AT 0Gy	42	18 (0.429)	13 (0.310)	5 (0.119)
AT 1Gy	191	179 (0.937)	132 (0.691)	47 (0.246)
Total	**233**	**197 (0.846)**	**145 (0.622)**	**52 (0.223)***
Normal 0Gy	61	15 (0.246)	12 (0.197)	3 (0.049)
Normal 1Gy	215	94 (0.438)	79 (0.367)	15 (0.070)
Total	**276**	**109 (0.395)**	**91 (0.330)**	**18 (0.065)***

* χ^2 test: $p<0.05$. Frequency of breaks is based on the total number of cells analysed.

TITLES AND LEGENDS TO FIGURES

Figure 1

A. **Exchange type *vs* non-exchange type aberrations**. **I, II and III:** Fragments of metaphases carrying exchange type aberrations obtained from normal cells at 71h after 1Gy irradiation. On the mFISH images (left) arrowheads signal reciprocal translocations (t). The capping status of these translocations is shown in the telomeric & centromeric image (right). All translocations shown are correctly capped and possess four telomeric signals. **I**: t(6;8) involving chromosomes 6 (green) and 8 (red). **II**: t(2;4) involving chromosomes 2 (red) and 4 (brown-green). **III**: t(6;11) involving chromosomes 6 (green) and 11 (light blue). **IV, V and VI:** Fragments of metaphases carrying open, non-exchange type aberrations obtained from AT cells at 71h p.i. **IV**: Arrowheads on the mFISH image (left) show two fragments of chromosome 6 (green). Arrowheads on the telomeric & centromeric image mark the broken centromeric fragment of chromosome 6 (top left) that lacks two telomeric signals. The corresponding acentric fragment of chromosome 6 with a single pair of telomeric signals is found in the same image (bottom right). **V**: Arrowheads in the mFISH image show two fragments corresponding to chromosome 4 (brown-green). Arrowheads in the telomeric & centromeric image show the broken centromeric fragment of chromosome 4 (left) and the corresponding acentric fragment (right), both with a single pair of telomeres. **VI**: Arrowheads in the mFISH image show a compound fragment of chromosomes 7 and 11 and a fragment of chromosome 11 (top left). Arrowheads in the telomeric & centromeric image show a broken dicentric (7;11) that lacks two telomeric signals on the end corresponding to chromosome 11 (bottom left) and an acentric fragment (top left) corresponding to chromosome 11. **B. Frequency of Exchange type aberrations (Ex Ab) *vs* Non-exchange type aberrations (Non-Ex Ab).** At 71 hours after 1Gy irradiation, extreme radiosensitive AT cells present double frequency of aberrations per cell than irradiated normal cells. Most aberrations scored in both cell types are of the exchange-type, but AT cells present 4 times more aberrations belonging to the non-exchange type group than normal cells (*statistically significant difference). **C: Detailed**

frequency of all types of aberrations in normal and AT cells at 71h after 1Gy irradiation: t: translocations; **dic**: dicentrics; **R-id**: rejoined interstitial deletions; **UR-id**: unrejoined interstitial deletions; **csb-del**: chromosome breaks and terminal deletions. A detailed observation of the different aberration types reveals that, while almost all aberrations are 1.5 to 2 times more frequently found in irradiated AT cells, chromosome breaks and terminal deletions present an outstanding difference, being 7 times more frequent in irradiated AT cells than in irradiated normal cells (*statistically significant difference).

Figure 1

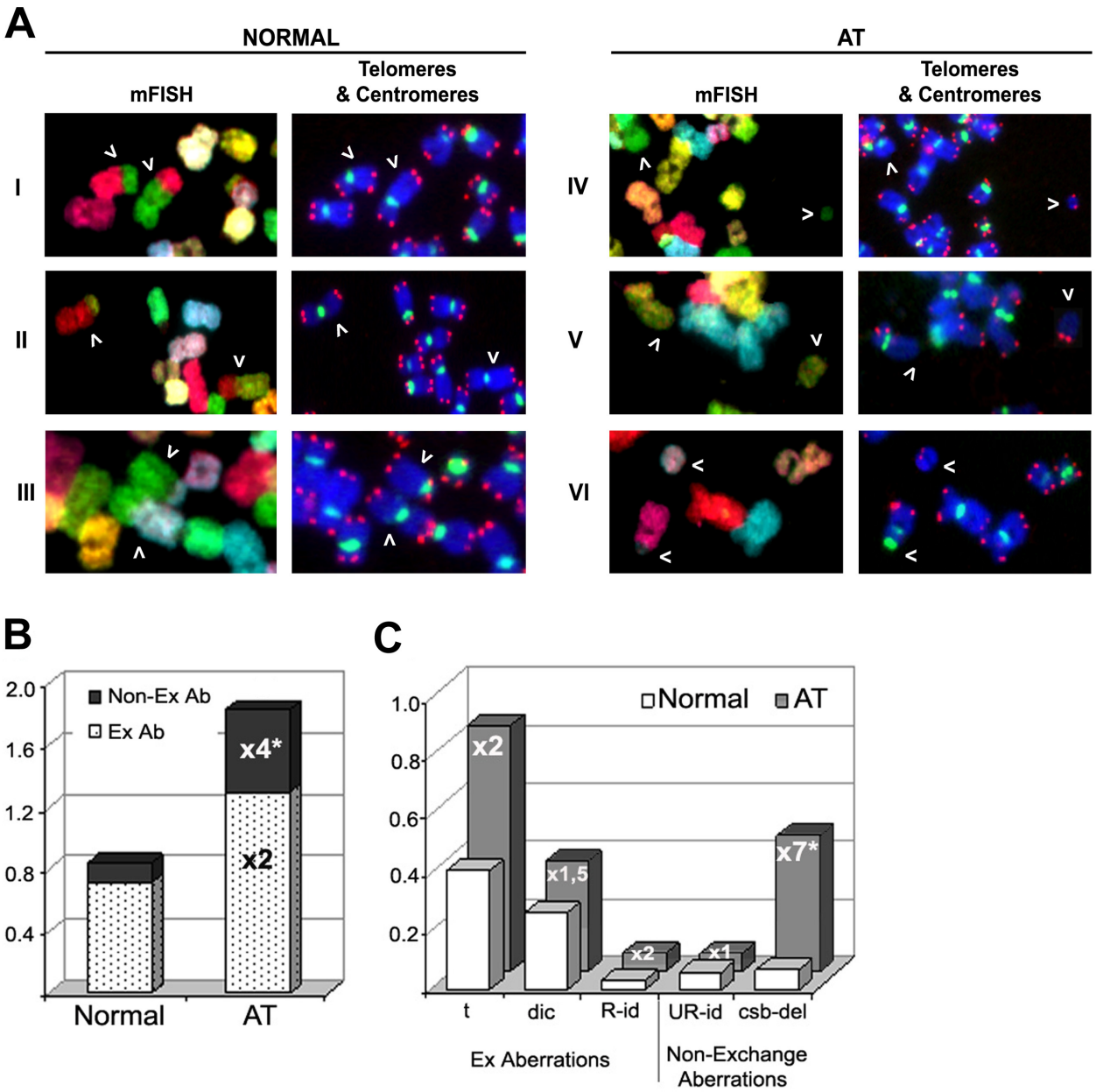
A
NORMAL
AT
mFISH
Telomeres & Centromeres
mFISH
Telomeres & Centromeres
I
II
III
IV
V
VI
B
2.0
1.6
1.2
0.8
0.4
Non-Ex Ab
Ex Ab
x4*
x2
Normal
AT
C
1.0
0.8
0.6
0.4
0.2
Normal
AT
x2
x1,5
x2
x1
x7*
t
dic
R-id
UR-id
csb-del
Ex Aberrations
Non-Exchange Aberrations

Figure 2

A. SCF event detection. True SCF events: Possible SCF events were detected using coded slides from normal and AT cells at first division after 1Gy irradiation. First, slides were Leishman stained and chromosomes presenting rounded, presumably sealed ends (arrowheads) were annotated (left). After telomeric & centromeric FISH (right), the SCF events were confirmed if the previously scored rounded ends were devoid of a telomeric pair. **False SCF events**: A fraction of the possible SCF events scored during Leishman staining analysis (arrowheads) were discarded after the telomeric & centromeric FISH because of the presence of telomeres at the rounded end. **B. Formation of isodicentric and isoacentric figures after SCF:** A chromosome is broken during **G1** and reaches the **S/G2** phase without being repaired. During S phase, the broken chromatid replicates and the broken sister chromatids can fuse (**SCF**). When this figure reaches **mitosis** (**M**) and begins anaphase, cohesins along the chromosome arms will be destroyed and the two centromeres will be pulled to opposite poles. Thus, segregation of the broken centromeric fragment in the next division can take place with or without breakage. If the centromere pulling results in breakage, a one-chromatid broken chromosome will be found in the G1 phase of the next division (b). If segregation resolves without breakage, a one-chromatid isodicentric will be found in the **G1** phase of the **next division** (c). The acentric fragment is not pulled to opposite poles during mitosis, so -if segregated- an intact one-chromatid acentric fragment will be found at G1 in one of the daughter cells (d). The banding pattern of the iso-figures will be a mirror image converging in the chromatid-fusion point. After entering S phase, chromatids will replicate again. Therefore, when the cell reaches the second mitosis after irradiation, inverted duplications, deletions, isodicentric chromosomes and isoacentric fragments can all be found in the metaphase spreads. **C: Iso-figure in irradiated AT cells**. From left to right: *Inverted DAPI image*: three chromosomes can be seen in this image; a normal chromosome 6 (left), a deleted centric fragment of 6q (middle), and a duplication of the 6p acentric fragment (right). The mirror-banding pattern is evident in this 6p duplicated fragment

(arrowhead). *Centromeric and telomeric hybridization image*: The 6p iso-fragment (right) is perfectly capped and four telomeres are scored. Finally, the *mFISH image* allows us to conclude that all figures implicated correspond to chromosome 6, thus discarding small translocations or other exchange type events.

Figure 2

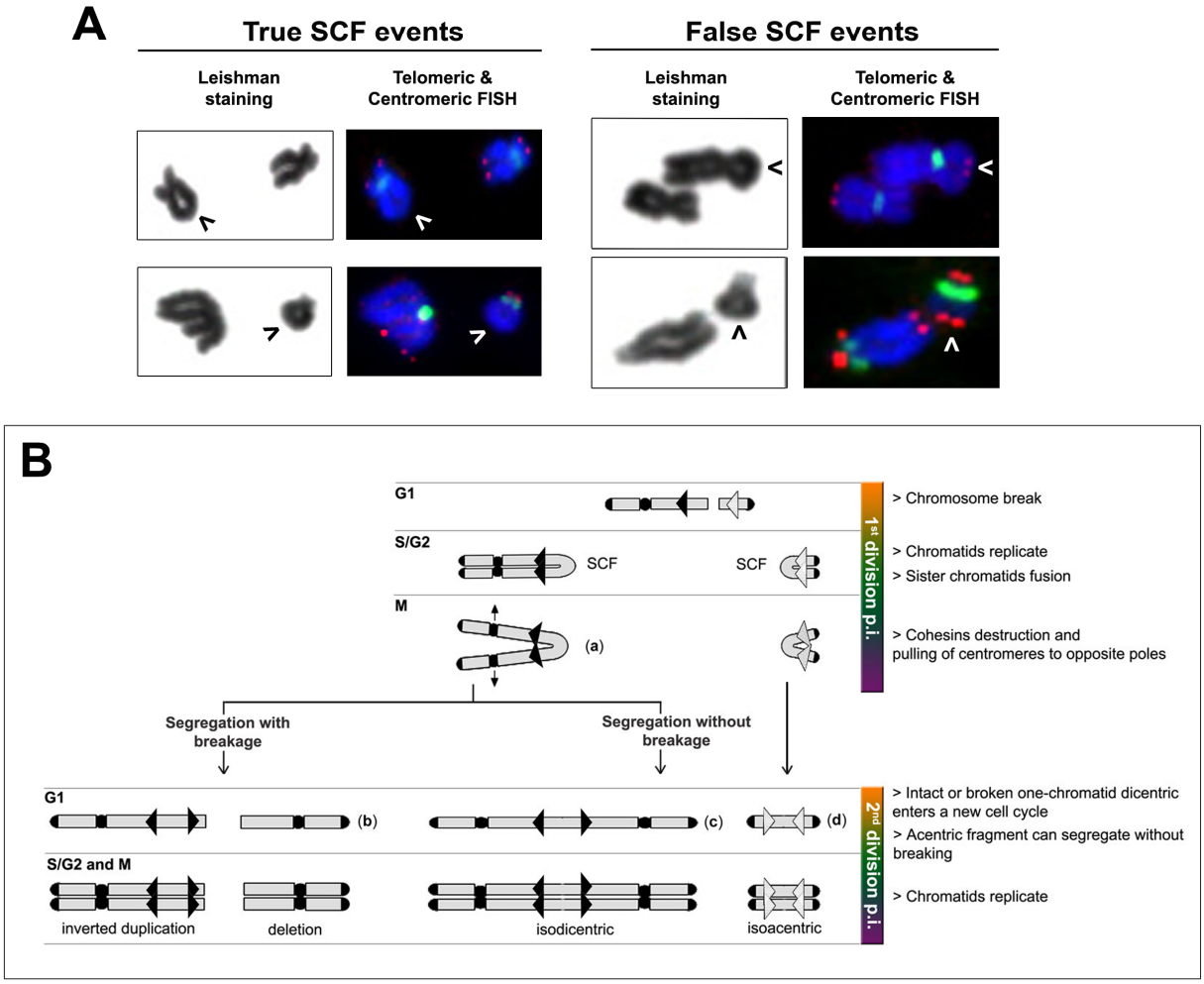
A
True SCF events
False SCF events
Leishman staining
Telomeric & Centromeric FISH
Leishman staining
Telomeric & Centromeric FISH
B
G1
S/G2
M
SCF
SCF
(a)
> Chromosome break
> Chromatids replicate
> Sister chromatids fusion
> Cohesins destruction and pulling of centromeres to opposite poles
1st division p.i.
Segregation with breakage
Segregation without breakage
G1
(b)
(c)
(d)
S/G2 and M
inverted duplication
deletion
isodicentric
isoacentric
> Intact or broken one-chromatid dicentric enters a new cell cycle
> Acentric fragment can segregate without breaking
> Chromatids replicate
2nd division p.i.
C
Inverted DAPI
Telomeric & Centromeric hybridization
mFISH
6
6
6

Figure 3

DSB repair kinetics for irradiated AT and normal cells. **A:** Typical asymmetrical FIGE gels corresponding to the DSB rejoining kinetics from normal and AT cells. Both cell types were irradiated at 30Gy and the repair rate was measured at 0, 0.5, 1, 2, 4, 8 and 24 hours after irradiation. The repair rate for each time analysed was measured using the FAR (Fraction of Activity Released) value: fraction of DNA released to the gel lane compared to the total DNA (well + lane). **B:** The values for time 0 after irradiation (arrowhead) are very similar for normal and AT cells, demonstrating that the initial radio-inflicted damage is almost the same for both cell lines. Overall, the repair rate in the first 8 hours is very similar for both cell lines. Twenty-four hours after irradiation AT cells have not reached complete repair, and the FAR value remains the same as at previous points in time. Circles: mean of two determinations from three independent experiments; bars: SD.

Figure 3

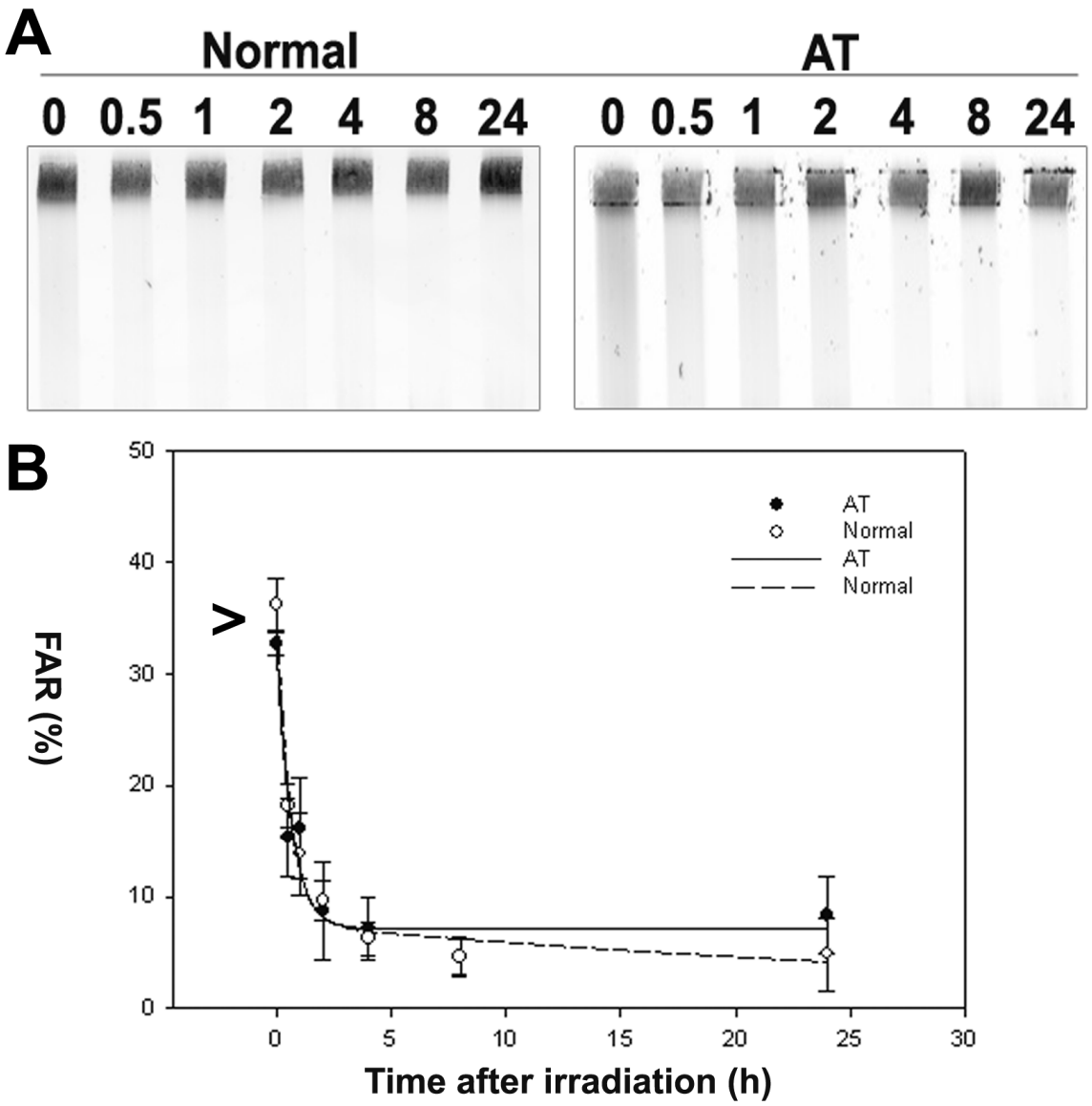
A
Normal
AT
0 0.5 1 2 4 8 24
0 0.5 1 2 4 8 24
B
FAR (%)
Time after irradiation (h)
AT
Normal
AT
Normal
0
10
20
30
40
50
0
5
10
15
20
25
30

Figure 4

A. Breaks with and without histone labelling. (From top to bottom) **Break detection**: After 1Gy irradiation a telomeric probe is applied to AT and normal cells slides in order to detect chromosome breaks (highlighted with square insets). A schematic representation of the affected broken chromosomes is found on the right of every photograph. **γH2AX detection**: After detecting the break, γH2AX-immunostaining is performed on the same slides. Both γH2AX-labelled and unlabelled breaks were scored. **Merged**: merged image where telomeres and γH2AX labelling at the breakpoint (if present) can be seen. **B. γH2AX detection and mFISH hybridization.** On some irradiated slides (1Gy), mFISH was applied after γH2AX detection**. γH2AX-labelled fragments of a broken chromosome. Break detection**: metaphase extension where two broken chromosome fragments are detected (arrowheads) after applying telomeric FISH. One of the chromosome breaks (bottom left) is a large chromosome fragment while the other (top right) is a very small chromosome fragment. Both fragments present a single pair of telomeric signals. **γH2AX detection**: After immunostaining, both chromosome fragments present γH2AX labelling (green) at the break point (arrowheads). **Identification of chromosomes**: After mFISH hybridization, the metaphase is karyotyped. Both fragments correspond to the centromeric and acentric fragment of a broken chromosome 8. The intact homologue chromosome 8 was also found on the metaphase. **γH2AX-unlabelled fragments of a broken chromosome. Break detection**: metaphase extension where a chromosome break with a single telomeric pair is detected (arrowhead). **γH2AX detection**: After immunostaining, the small chromosome fragment does not present γH2AX labelling (green) at the breakpoint (arrowheads). **Identification of chromosomes**: After mFISH hybridization, the chromosomes involved in the aberration are identified. The acentric chromosome fragment corresponds to a piece of chromosome 4. Two intact chromosomes 4 were also found in the metaphase and are shown in the image. These intact chromosomes possess two telomeric pairs each and do not present any visible chromatid break, indicating that this acentric fragment most probably

originated in a previous cell division, and has been segregated in an unrepaired status. **C. Diagram** showing the outcomes obtained from irradiated (1Gy) and non-irradiated cells computed together. As expected, frequency of total breaks is more than double in AT than in normal cells. While breaks signalled with histone (green) are the most frequent breaks in both cell lines, breaks devoid of histone signal (red) are strikingly more frequent in AT cells (*statistically significant difference).

Figure 4

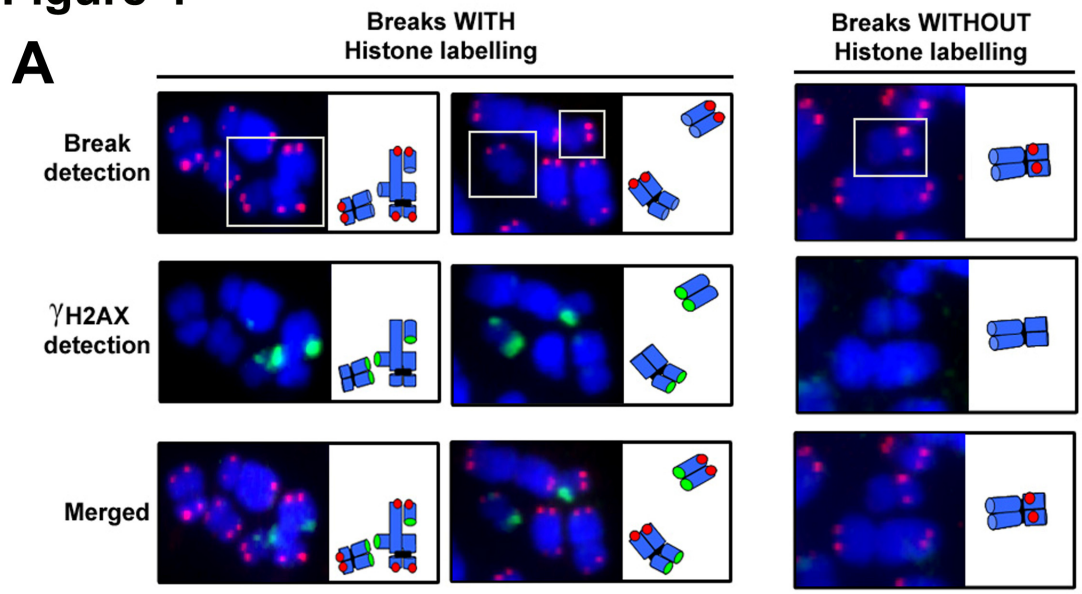
A
Breaks WITH Histone labelling
Breaks WITHOUT Histone labelling
Break detection
γH2AX detection
Merged

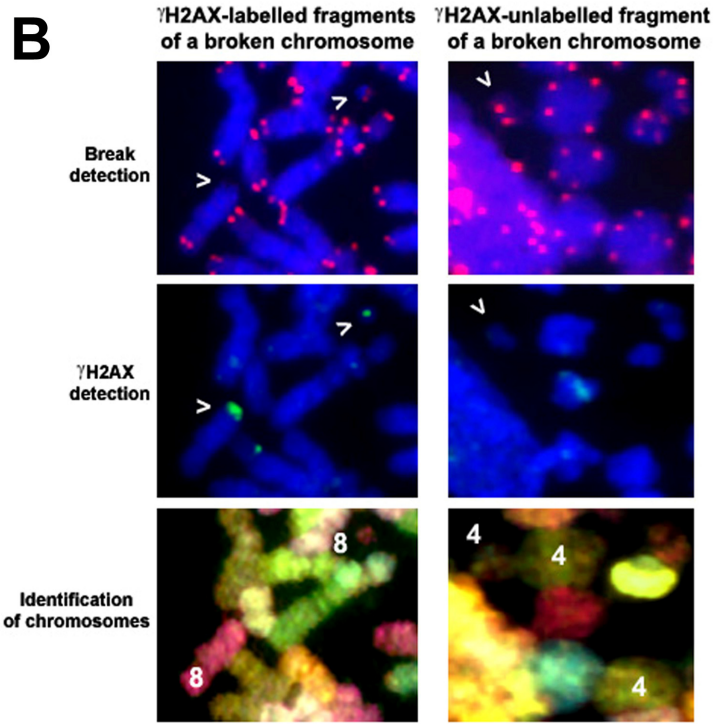
B
γH2AX-labelled fragments of a broken chromosome
γH2AX-unlabelled fragment of a broken chromosome
Break detection
γH2AX detection
Identification of chromosomes
8
8
4
4
4

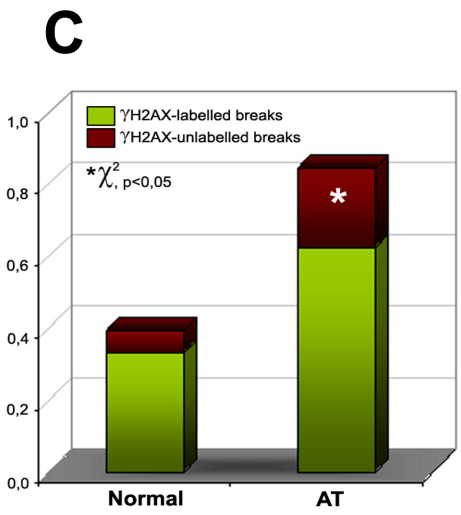
C
γH2AX-labelled breaks
γH2AX-unlabelled breaks
*χ², p<0,05
1,0
0,8
0,6
0,4
0,2
0,0
Normal
AT

Figure 5.

A. γH2AX- and Mre11-labelled break: Chromatid breaks were clearly identified after DAPI staining of metaphase spreads from 1Gy irradiated AT and normal cells (>). Most of the scored breaks in both cell types presented a γH2AX (green) focus at the breakpoint. The γH2AX focus at the breakpoint always co-localized with an Mre11 (red) focus, which are seen as yellow foci in the merged image. **γH2AX- and Mre11-unlabelled break:** All breaks scored devoid of γH2AX focus also lacked any Mre11 labelling (*), suggesting that repair proteins are not present at γH2AX-unlabelled breaks. **B. Diagram** showing distribution of γH2AX- and Mre11-labelling status of scored breaks in irradiated AT and normal cells. In neither cell line breaks displaying only γH2AX-labelling or only Mre11-labelling were present.

Figure 5

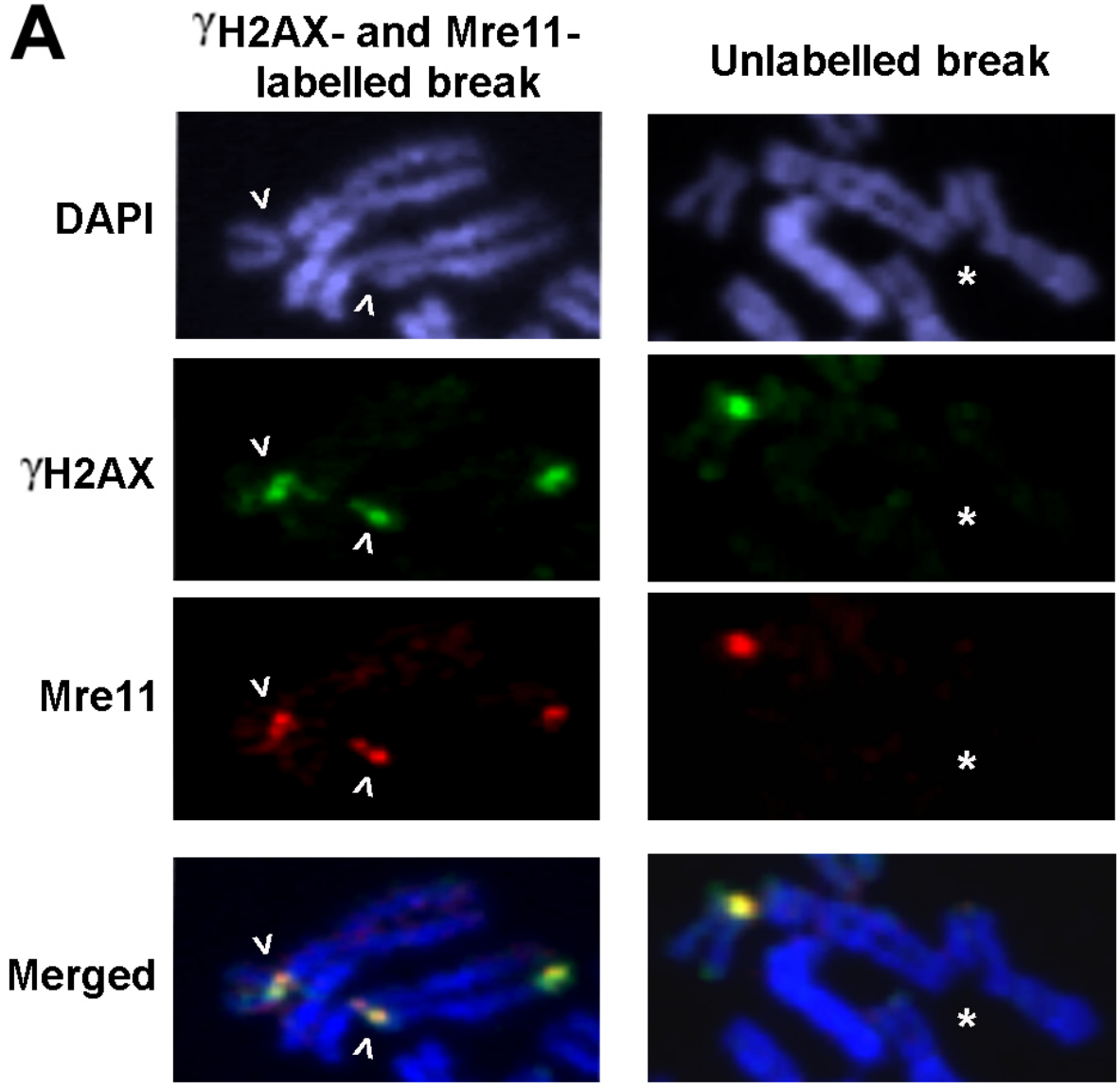
A
γH2AX- and Mre11-labelled break
Unlabelled break
DAPI
γH2AX
Mre11
Merged
B
γH2AX- and Mre11-labelled breaks (>)
γH2AX- and Mre11-unlabelled breaks (*)
Number of breaks
0
10
20
30
40
50
60
Normal
AT

BIBLIOGRAPHY

Abraham RT, Tibbetts RS. 2005. Guiding ATM to Broken DNA. Science 308, 510-511.

Blöcher D, Sigut D, Hannan MA. 1991. Fibroblasts from ataxia telangiectasia (AT) and AT Heterozygotes show an enhanced level of residual DNA double-strand breaks after low dose-rate gamma-irradiation as assayed by pulsed field gel electrophoresis. International Journal of Radiation Biology 60, 791-802.

Bredemeyer AL, Huang C-Y, Walker LM, Bassing CH, Sleckman BP. 2008. Aberrant V(D)J Recombination in ataxia telangiectasia mutated-deficient lymphocytes is dependent on nonhomologous DNA end joining. J Immunol 181, 2620-2625.

Bredemeyer AL, Sharma GG, Huang C-Y, Helmink BA, Walker LM, Khor KC, Nuskey B, Sullivan KE, Pandita TK, Bassing CH, Sleckman BP. 2006. ATM stabilizes DNA double-strand-break complexes during V(D)J recombination. 442, 466-470.

Burma S, Chen BP, Murphy M, Kurimasa A, Chen DJ. 2001. ATM phosphorylates histone H2AX in response to DNA double-strand breaks. J Biol Chem 276, 42462-42467.

Callen E, Jankovic M, Difilippantonio S, Daniel JA, Chen H-T, Celeste A, Pellegrini M, McBride K, Wangsa D, Bredemeyer AL. 2007. ATM prevents the persistence and propagation of chromosome breaks in lymphocytes. Cell 130, 63-75.

Celeste A, Fernandez-Capetillo O, Kruhlak MJ, Pilch DR, Staudt DW, Lee A, Bonner RF, Bonner WM, Nussenzweig A. 2003. Histone H2AX phosphorylation is dispensable for the initial recognition of DNA breaks. Nature Cell Biology 5, 675-679.

Cornforth MN, Bedford J. 1985. On the nature of a defect in cells from individuals with ataxia-telangiectasia. Science 29, 1589-1591.

Foray N, Priestley A, Alsbeih G, Badie C, Capulas E, Arlett C, Malaise E. 1997. Hypersensitivity of ataxia telangiectasia fibroblasts to ionizing radiation is associated with a repair deficiency of DNA double-strand breaks. International Journal of Radiation Biology 72, 271-283.

Franco S, Gostissa M, Zha S, Lombard DB, Murphy MM, Zarrin AA, Yan C, Tepsuporn S, Morales JC, Adams MM. 2006. H2AX prevents DNA breaks from progressing to chromosome breaks and translocations. Molecular Cell 21, 201-214.

Goodarzi AA, Noon AT, Deckbar D, Ziv Y, Shiloh Y, Löbrich M, Jeggo PA. 2008. ATM Signaling facilitates repair of DNA double-strand breaks associated with heterochromatin. Molecular Cell 31, 167-177.

Ichijima Y, Sakasai R, Okita N, Asahina K, Mizutani S, Teraoka H. 2005. Phosphorylation of histone H2AX at M phase in human cells without DNA damage response. Biochemical and Biophysical Research Communications 336, 807-812.

Jeggo PA, Lobrich M. 2005. Artemis links ATM to double strand break rejoining. Cell Cycle 4, 359-362.

Jeppesen P. 2000. Immunofluorescence in cytogenetic analysis:method and applications. Genetics and Molecular Biology 23, 1107-1114.

Karlsson KH, Stenerlöw B. 2004. Focus formation of DNA repair proteins in normal and repair-Deficient cells irradiated with high-LET ions. Radiation Research, 517-527.

Kato TA, Nagasawa H, Weil MM, Little JB, Bedford JS. 2006. Levels of gamma-H2AX foci after low-dose-rate irradiation reveal a DNA DSB rejoining defect in cells from human ATM heterozygotes in two AT families and in another apparently normal individual. Radiation Research, 443-453.

Kawata T, Ito H, George K. Wu H, Uno T, Isobe K, Cucinotta FA. 2003. Radiation-induced chromosome aberrations in ataxia telangiectasia cells: High frequency of deletions and misrejoining detected by fluorescence in situ hybridization. Radiation Research, 597-603.

Krempler A, Deckbar D, Jeggo PA, Lobrich M. 2007. An imperfect G2/M checkpoint contributes to chromosome instability following irradiation of S and G2 phase cells. Cell Cycle 6, 1682-1686.

Kühne M, Riballo E, Rief N, Rothkamm K, Jeggo PA, Lobrich M. 2004. A double-strand break repair defect in ATM-deficient cells contributes to radiosensitivity. Cancer Res 64, 500-508.

Kurz EU, Lees-Miller SP. 2004. DNA damage-induced activation of ATM and ATM-dependent signaling pathways. DNA Repair 3, 889-900.

Lavin MF. 2007. ATM and the Mre11 complex combine to recognize and signal DNA double-strand breaks. 26, 7749-7758.

Lee J-H, Paull TT. 2007. Activation and regulation of ATM kinase activity in response to DNA double-strand breaks. 26, 7741-7748.

Lo AWI, Sabatier L, Fouladi B, Pottier G, Ricoul M, Murnane JP. 2002a. DNA amplification by Breakage/Fusion/Bridge cycles initiated by spontaneous telomere loss in a human cancer cell line. Neoplasia 4, 531-538.

Lo AWI, Sprung CN, Fouladi B, Pedram M, Sabatier L, Ricoul M, Reynolds GE, Murnane JP. 2002b. Chromosome instability as a result of double-strand breaks near telomeres in mouse embryonic stem cells. Mol Cell Biol 22, 4836-4850.

Löbrich M, Kühne M, Wetzel J, Rothkamm K. 2000. Joining of correct and incorrect DNA double-strand break ends in normal human and ataxia telangiectasia fibroblasts. Genes, Chromosomes and Cancer 27, 59-68.

MacPhail S, Banáth J, Yu T, Chu E, Lambur H, Olive P. 2003. Expression of phosphorilated histone H2AX in cultured cell lines following exposure to X-rays. Int J Radiat Biol 79, 351-358.

Martín M, Genescà A, Latre L, Jaco I, Taccioli GE, Egozcue J, Blasco MA, Iliakis G, Tusell L. 2005. Postreplicative joining of DNA double-strand breaks causes genomic instability in DNA-PKcs-deficient mouse embryonic fibroblasts. Cancer Res 65, 10223-10232.

Martín M, Genescà A, Latre L, Ribas M, Miró R, Egozcue J, Tusell L. 2003. Radiation-induced chromosome breaks in ataxia-telangiectasia cells remain open. International Journal of Radiation Biology 79, 203-210.

McManus KJ, Hendzel MJ. 2005. ATM-dependent DNA damage-independent mitotic phosphorylation of H2AX in normally growing mammalian Cells. Mol Biol Cell 16, 5013-5025.

Niewolik D, Pannicke U, Lu H, Ma Y, Wang L-CV, Kulesza P, Zandi E, Lieber MR, Schwarz K. 2006. DNA-PKcs Dependence of Artemis endonucleolytic activity, differences between hairpins and 5' or 3' overhangs. J Biol Chem 281, 33900-33909.

Paull TT, Rogakou EP, Yamazaki V, Kirchgessner CU, Gellert M, Bonner WM. 2000. A critical role for histone H2AX in recruitment of repair factors to nuclear foci after DNA damage. Current Biology 10, 886-895.

Riballo E, Kuhne M, Rief N, Doherty A, Smith GCM, Recio M-J, Reis C, Dahm K, Fricke A, Krempler A. 2004. A pathway of double-strand break rejoining dependent upon ATM, Artemis, and proteins locating to gamma-H2AX foci. Molecular Cell 16, 715-724.

Rogakou EP, Boon C, Redon C, Bonner WM. 1999. Megabase chromatin domains involved in DNA double-strand breaks in vivo. J Cell Biol 146, 905-916.

Rogakou EP, Pilch DR, Orr AH, Ivanova VS, Bonner WM. 1998. DNA double-stranded breaks induce histone H2AX phosphorylation on Serine 139. Journal of Biological Chemistry 273, 5858-5868.

Rothkamm K, Lobrich M. 2003. Evidence for a lack of DNA double-strand break repair in human cells exposed to very low x-ray doses. Proceedings of the National Academy of Sciences 100, 5057-5062.

Sedelnikova OA, Rogakou EP, Panyutin IG, Bonner WM. 2002. Quantitative detection of 125IdU-induced DNA double-strand breaks with gamma-H2AX antibody. Radiation Research, 486-492.

Shiloh Y. 2006. The ATM-mediated DNA-damage response: taking shape. Trends in Biochemical Sciences 31, 402-410.

Stiff T, O'Driscoll M, Rief N, Iwabuchi K, Lobrich M, Jeggo PA. 2004. ATM and DNA-PK function redundantly to phosphorylate H2AX after exposure to ionizing radiation. Cancer Res 64, 2390-2396.

Ward IM, Minn K, Jorda KG, Chen J. 2003. Accumulation of checkpoint protein 53BP1 at DNA breaks involves its binding to phosphorylated histone H2AX. J Biol Chem 278, 19579-19582.

Williams RS, Williams JS, Tainer JA. 2007. Mre11-Rad50-Nbs1 is a keystone complex connecting DNA repair machinery, double-strand break signaling, and the chromatin template. Biochem Cell Biol 85, 509-520.